Ultra Strong Silicon-Coated Carbon Nanotube Nonwoven Fabric as a Multifunctional Lithium-Ion Battery Anode

Kara Evanoff,[†,‡] Jim Benson,[†] Mark Schauer,[§] Igor Kovalenko,[†] David Lashmore,[§] W. Jud Ready,[†,‡] and Gleb Yushin[†,*]

[†]School of Materials Science and Engineering, Georgia Institute of Technology, Atlanta, Georgia 30332-0245, United States, [‡]Electro-Optical Systems Laboratory, Georgia Tech Research Institute, Atlanta, Georgia 30332-0810, United States, and [§]Nanocomp Technologies, Inc., Concord, New Hampshire 03301, United States

ABSTRACT Materials that can perform simultaneous functions allow for reductions in the total system mass and volume. Developing technologies to produce flexible batteries with good performance in combination with high specific strength is strongly desired for weight- and power-sensitive applications such as unmanned or aerospace vehicles, high-performance ground vehicles, robotics, and smart textiles. State of the art battery electrode fabrication techniques are not conducive to the development of multifunctional materials due to their inherently low strength and conductivities. Here, we present a scalable method utilizing carbon nanotube (CNT) nonwoven fabric-based technology to develop flexible, electrochemically stable (~494 mAh·g^{-1} for 150 cycles) battery anodes that can be produced on an industrial scale and demonstrate specific strength higher than that of titanium, copper, and even a structural steel. Similar methods can be utilized for the formation of various cathode and anode composites with tunable strength and energy and power densities.

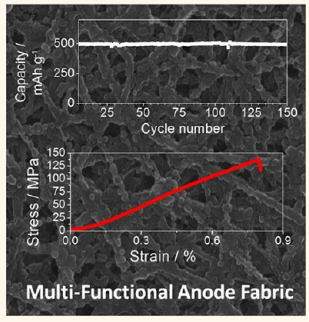

KEYWORDS: batteries · composite materials · multifunctional materials · electrodes · silicon

Multifunctional materials capable of providing an energy storage ability coupled with a load-bearing ability are attractive for applications in which reducing the overall mass and volume of equipment is important, such as for unmanned or aerospace vehicles[1−4] and high-performance equipment for commercial, professional, and military applications. Flexible Li-ion batteries with load-bearing abilities could be attractive candidates for these applications due to their high energy and power densities. As a first step toward realization of such a battery design, one needs to develop scalable synthesis routes to produce structural and flexible anodes and cathodes.

The traditional technique to fabricate electrodes requires mixing of the active particles with carbon conductive additives and a polymer binder and then casting of the mixture onto metal foil or mesh current collectors (Figure 1a). Due to numerous point contacts between the individual particles, the electrical and thermal conductivities of such traditional electrodes are quite limited.[5] The tensile strength of traditional electrodes is primarily dominated by the mechanical properties of the metal foil current collectors (Cu, Al) because the particles in the electrode are weakly bonded. Another disadvantage of traditional electrodes is the significant weight of the metal current collectors, which further limits the gravimetric capacities of the battery cells. For example, while commercial graphites exhibit capacities in the range of 300−360 mAh·g^{-1} and the weight of the binder and carbon additives is limited to only 10−15 wt %, the effective capacities of Li-ion battery anodes are commonly less than 200 mAh·g^{-1} if all of the materials including heavy Cu foil are taken into account. Indeed, the weight of the Cu foil accounts for over 35% of the total weight. If high capacity Li-alloying materials such as silicon (Si) are used to improve the gravimetric energy density of Li-ion batteries,[5−18] then the relative weight of the Cu foil may account for up to 80 wt %.

Various approaches to fabricate structural electrodes to enhance the mechanical

* Address correspondence to yushin@gatech.edu.

Received for review July 27, 2012 and accepted October 17, 2012.

Published online October 17, 2012
10.1021/nn303393p

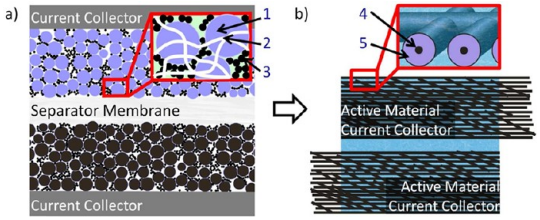

Figure 1. Schematics of elementary Li-ion battery units for (a) traditional and (b) proposed architectures. In a traditional architecture, the electrodes, composed of active powders (1), polymer binder (2), and conductive carbon additives (3), are cast on metal current collector foils. In a proposed architecture, CNT fabric (4) coated with active material layers (5) serves as lightweight multifunctional current collector for both anodes and cathodes.

properties have been reported in the literature.[2,3,19−21] Following traditional electrode fabrication techniques, a previous study combined $LiCoO_2$ particles, carbon additives, and polymer binder into a slurry and measured a maximum tensile strength <5 MPa, a value which may limit widespread applicability of this technique to provide structural support due to the low polymer binder strength and its low content.[2] Sintered composite particle-based electrodes demonstrated increased strength (~90 MPa); however, the capacity retention over 10 cycles was very poor with only 85% of the theoretical capacity retained.[3] In addition, the sintered electrodes are not flexible, which may limit some of their multifunctional applications.

Flexible electrodes comprising graphene or carbon nanotubes (CNTs) may offer excellent thermal, electrical, and mechanical properties[22] that may be additionally enhanced through post-synthesis treatments.[23−26] Graphene paper electrodes have demonstrated very high tensile strength of up to 290 MPa; however, such electrodes suffer from poor cycling ability, very low first cycle Coulombic efficiency (CE) of ~12%, and low reversible capacity of ~55 $mAh \cdot g^{-1}$, metrics much lower than traditional graphite electrodes.[21,27] Insertion of electrolyte solvent molecules between the individual graphene sheets and their decomposition may explain the observed rapid degradation.[17,28−30] One may further expect that the mechanical properties of such electrodes should also degrade dramatically after electrochemical cycling. Although tensile tests of individual multiwalled CNTs (MWCNTs) have previously shown tensile strengths >11 GPa,[31] this value is several orders of magnitude higher than the tensile strengths observed for nonwoven CNT fabrics and CNT-polymer composites.[19,20,32−34] Commonly reported methods of forming CNT fabrics or buckypapers rely on vacuum filtration of acid-treated CNTs,[34,35] impregnation with a polymer,[33,36] or the addition of surfactant[32] to form a fabric with limited size, typically less than a few inches in diameter. In these approaches, the ability to produce continuous rolls of the CNT fabric/paper with good mechanical strength is very limited and the batch-to-batch variability makes large-scale applications difficult. Furthermore, the insertion of electrolyte solvent molecules between the individual CNTs will likely result in high irreversible capacity losses and low CE at the first cycle combined with rapid degradation of such CNT electrodes if used as Li-ion battery anodes.

Here we report for the first time a route to produce flexible anodes with significantly higher strength and specific capacity than state of the art. According to our approach, we first produce a high-strength binder-free CNT-based electrically conductive nonwoven fabric and then coat it with a uniform layer of a high capacity material (Figure 1b) such as Si. Deposition of an active material on a preformed fabric shall allow one to maintain the high electrical and thermal conductivities of the composite because of the elimination of the highly resistive particle-to-particle contacts.[5] In contrast to common CNT fabric assembly methods, we utilize a commercial-scale continuous chemical vapor deposition (CVD) process. This method allows for the scalable production of multifunctional structural materials of various geometries. The deposited Si coating is impermeable to solvent molecules and protects the individual CNT−CNT junctions from failure during cycling. Furthermore, we limited the amount of inserted Li ions to prevent mechanical electrode degradation. Indeed, in contrast to previously reported studies,[32−34] we show high tensile strength of a composite Si-CNT fabric after electrochemical cycling with ultimate tensile strengths (UTS) greater than 90 MPa achieved. The electrochemical performance of the CNT fabric electrodes demonstrated stability for more than 150 cycles.

RESULTS AND DISCUSSION

The as-produced large format, flexible CNT fabric consists of randomly oriented MWCNTs as observed *via* scanning electron microscopy (SEM, Figure 2a). A conformal layer (~20 nm in thickness) of nano-Si was deposited on individual CNTs throughout the fabric (Figure 2b) *via* the thermal decomposition of SiH_4. Energy-dispersive X-ray spectroscopy (EDS) mapping indicates that the Si is uniformly deposited throughout the fabric (Figure S1 in Supporting Information). The CNT fabric retained its flexibility after Si deposition (Figure 2c,d). Although the CNT fabric is relatively thin (~20 μm), the energy density and specific energy of the battery will not be significantly compromised due to the incorporation of high capacity Si and the absence of a metal current collector.

Raman spectroscopy was performed on the CNT fabric before and after Si coating (Figure 3). The initial CNT fabric exhibits two strong Raman peaks at ~1320 and ~1590 cm^{-1}, corresponding to the D-band originating from disordered carbon and the G-band from graphitic carbon, respectively.[37,38] The low value of the

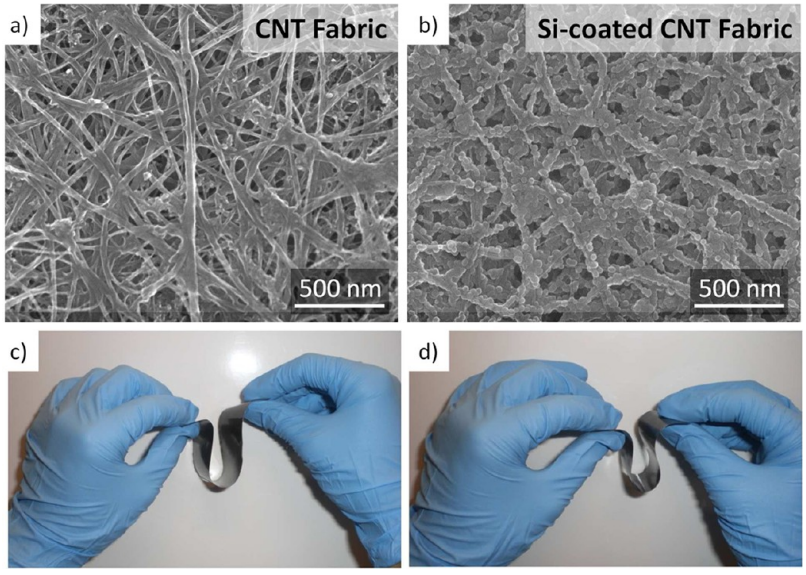

Figure 2. (a,b) SEM micrographs and (c,d) photographs of the CNT fabric (a,c) before and (b,d) after Si coating.

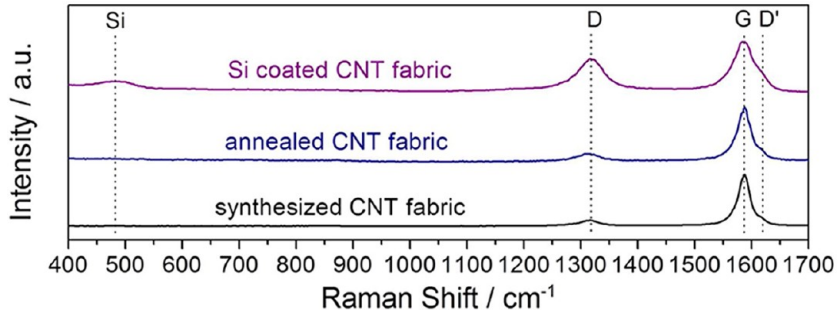

Figure 3. Raman spectra for the synthesized, annealed, and Si-coated CNT fabric.

ratio of the integrated intensities of the D- and G-bands, the I_D/I_G ratio, of 0.14 indicates a low defect density in the CNTs.[37−39] The slight asymmetry of the G-band is attributed to the D′-band at ∼1620 cm^{-1} and is present in all sample types analyzed.[37] To reveal the effect of thermal annealing during Si deposition, the CNT fabric was annealed in Ar under temperature and pressure conditions replicating Si deposition but in the absence of SiH_4. The annealed CNT fabric was found to also maintain a very low I_D/I_G value (0.18), indicating that significant changes to the microstructure due to thermal energy do not occur (Figure 3). After Si coating, a broad Raman band at ∼480 cm^{-1} associated with hydrogenated amorphous Si emerges[40,41] and the I_D/I_G ratio significantly increases to 0.82. The increased concentration of defects in CNTs is attributed to the free hydrogen produced as a SiH_4 decomposition product, which is known to induce surface defects in carbon at elevated temperatures.[42−44] Some defects may additionally form at the interface between the CNT and the Si coating upon cooling to relieve stress at the interface due to differences in thermal expansion coefficients. Both of these effects would give rise to higher intensity of the D-band.

Electrochemical measurements of the CNT fabric-based electrodes were performed in both pouch and 2016-type coin cell configurations against a metallic Li foil counter electrode in the voltage range from 0.01 to 1 V *vs* Li/Li^+ with a 500 mAh·g^{-1} (985 mAh·g_{Si}^{-1}, LiSi average composition) Li insertion capacity (Figure 4). The moderately high Li insertion capacity was selected as a compromise between high energy storage capability and good mechanical stability of the produced electrodes. Stable performance at C/5 was achieved for >150 cycles, suggesting good integrity of the composite anode. An average dealloying capacity of 494 mAh·g^{-1}(642 mAh·cm^{-3}), when normalized by the total mass of CNT and Si, and an average CE of ∼98% were observed (Figure 4a and Figure S2). This capacity is over 2.5 times higher than that of commercial electrodes based on graphite−binder mixtures deposited on Cu foils, demonstrating the promise of the proposed technology. The rate capability tests (Figure S3), however, showed very moderate performance at high current densities. These results suggest that in the current configuration the produced fabrics should primarily be used at medium-to-slow discharge rates.

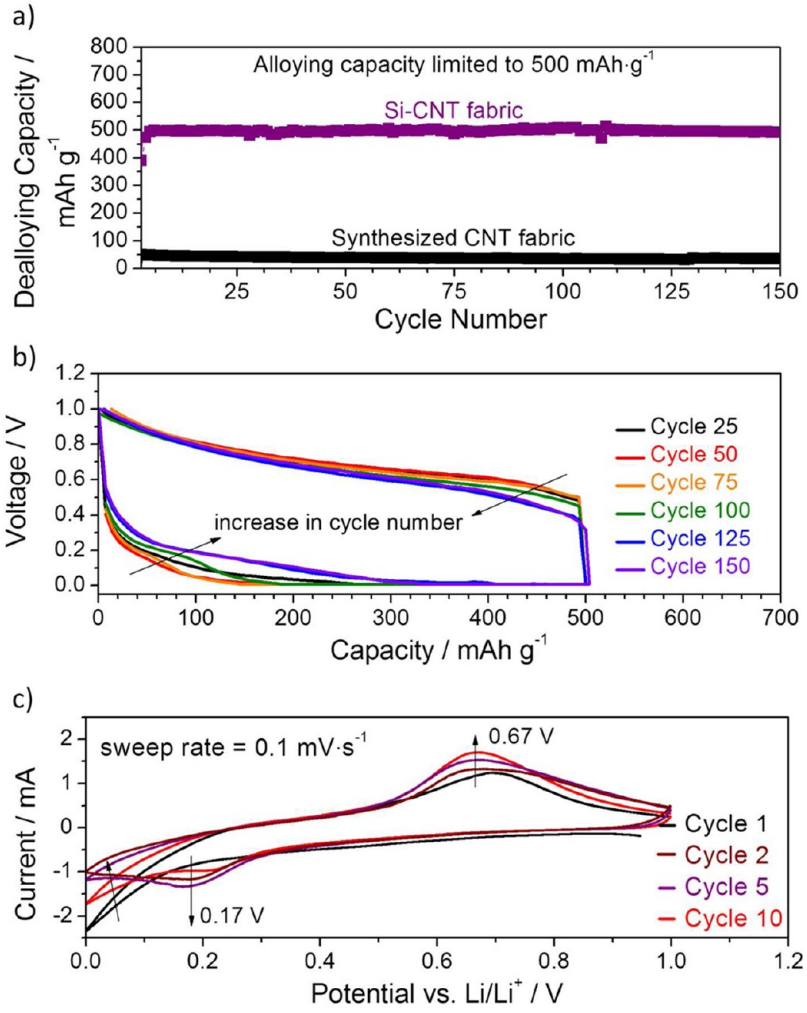

Figure 4. Electrochemical performance of Si-coated CNT fabric: (a) reversible dealloying (Li extraction) capacity *versus* cycle number in comparison to the synthesized CNT fabric; (b) changes in the charge and discharge profiles with cycle number; (c) cyclic voltammograms.

Charge/discharge voltage profiles of the Si-coated CNT fabric (Figure 4b) show transformations in the electrode during cycling. With increased cycling (>75 cycles), lower overpotentials were observed, indicating an improvement in cycling kinetics. Similarly, cyclic voltammetry (CV) was performed to further examine the potentials at which Li (de)alloying occurs (Figure 4c). A peak at 0.17 and 0.67 V emerged during lithiation and delithiation, respectively. These values are consistent with previous nanoscale Si-based composite anodes and indicate a high degree of alloying with Si.[5,7,8,45,46] CV does not show peaks corresponding to intercalation of Li into CNTs; however, they may be masked due to the significantly larger Li capacity of Si since the capacity is not limited in CV experiments and the CNT fabric (without Si) can only offer limited capacity (<10%) (Figure 4a). CV performed at a slower scan rate showed a slight shift in peak potentials, thus indicating that kinetics are not yet optimized for this structure (Figure S4).

Localized thermal and electrical gradients have been demonstrated to cause unbalanced charging and discharging that leads to premature aging of the battery.[47−50] In a traditional powder-based electrode, heat flows through the electrode to the current collector in the cross-plane direction.[49] For applications in which the current collector is removed, high in-plane thermal and electrical conductivities of the active material become critically important, thus the in-plane thermal and electrical conductivities for the CNT fabric before and after Si coating were measured (Table S1). In comparison to traditional powder-based electrodes based on Si nanopowder or graphite technology,[5,49,51] the thermal and electrical conductivities of CNT fabric-based electrodes show a 1−2 order of magnitude improvement in thermal conductivity and up to 5 order of magnitude reduction in electrical resistivity. The achieved ultrahigh thermal and electrical transport within the produced fabric highlights additional benefits of the proposed technology.

Uniaxial tensile test experiments were conducted on the CNT fabrics before and after battery cycling. The initial CNT fabric revealed very high maximum

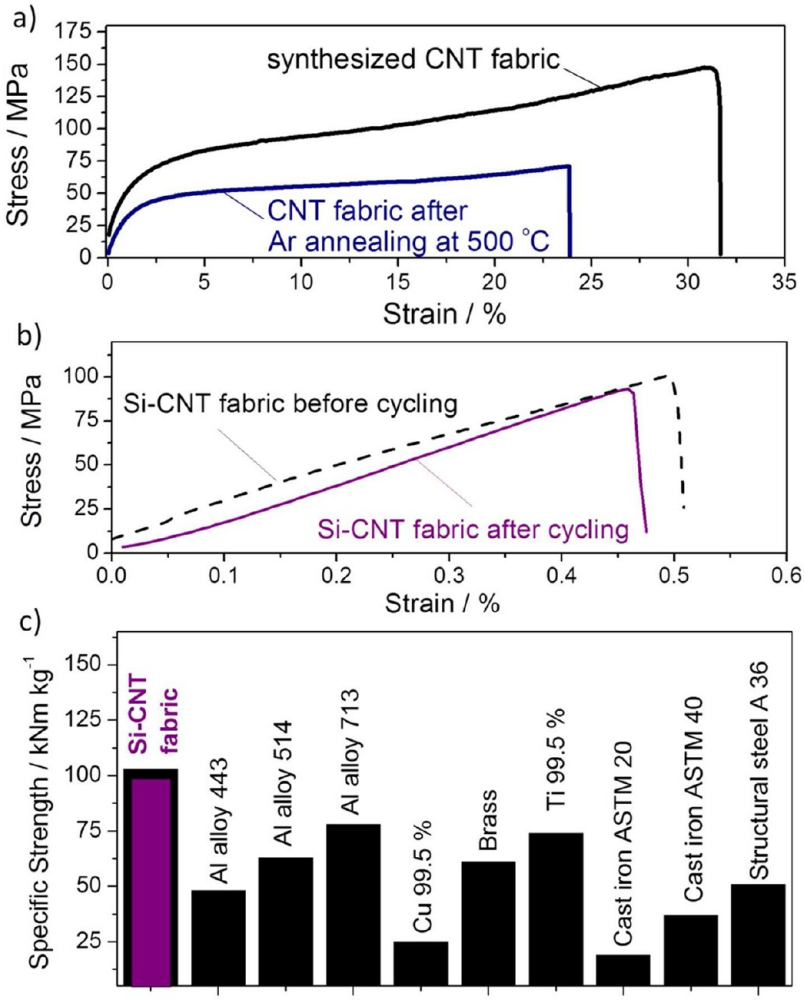

Figure 5. Mechanical characterization of the produced samples: (a) typical tensile tests on CNT fabric before and after annealing in Ar; (b) typical tensile tests on Si-coated CNT fabric before and after cycling; (c) comparison of the specific strength of the multifunctional Si-coated CNT fabric with that of other common materials.

elongations of over 30% and UTS value in excess of 150 MPa, comparable to that of cast iron, copper, and aluminum alloys[52] (Figure 5a), and up to 5 times higher than previously reported CNT sheets with[33,34] and without[19,20,32] polymer throughout. We shall note, however, that because of the limited porosity available within the produced fabrics for silicon expansion, cycling without insertion capacity limitation resulted in rapid mechanical and electrochemical degradation (Figure S5). Therefore, a balance between the porosity, utilized capacity, and the desired mechanical properties shall be carefully considered when designing multifunctional electrodes for future applications.

As the Si deposition process subjects the electrodes to 500 °C, it is important to study the impact of the heating process on the mechanical properties of the CNT fabric. Annealing the fabric at 500 °C in Ar reduces the maximum elongation to an average value of 24% and the UTS to ~55 MPa. Longer annealing time does not reduce the fabric mechanical properties any further, and 500 °C is sufficiently high to defunctionalize CNTs and possibly cause different pull-out behavior due to CNT realignment.

Thermogravimetric analysis (TGA) and X-ray photoelectron spectroscopy (XPS) were performed on synthesized and annealed CNT fabrics to confirm removal of functional groups. Analysis of the TGA derivative curve (Figure S6) for the synthesized CNT fabric shows significant mass losses occurring at temperatures <400 °C that can be associated with defunctionalization[53] and that are not seen in the annealed CNT fabric. This result is in good agreement with the XPS survey and high-resolution scans that show dramatic reductions in the O1s and N1s spectra after annealing (Figure S7). Comparison of the O/C and N/C atomic % ratios before and after annealing reveals reductions of 0.094 to 0.009 and 0.001 to 0, respectively. Removing the functional groups from the CNT surface leaves behind defects which may reduce the axial strength of the individual tubes.[53] In addition, removing these functional groups reduces the steric interactions between the tubes which allows only van der Waals bonding between

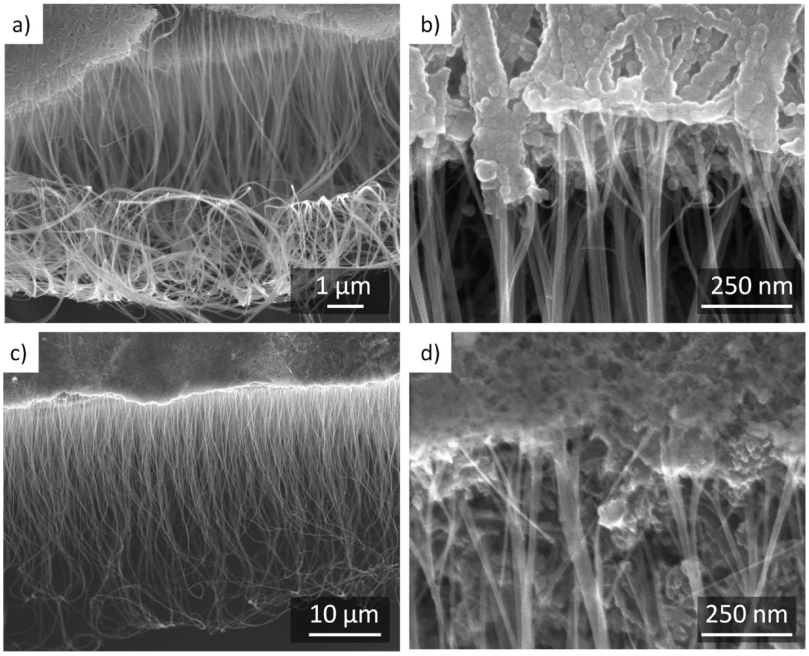

Figure 6. SEM micrographs of the fracture surface of the Si-coated CNT fabric edge after tensile measurements performed before (a,b) and after (c,d) electrochemical testing.

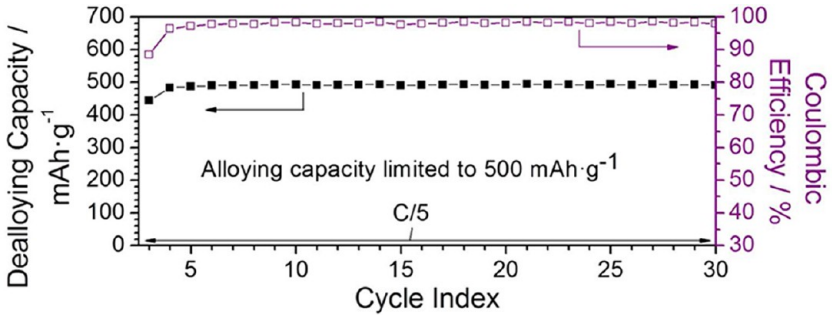

Figure 7. Reversible dealloying (Li extraction) capacity and Coulombic efficiency *versus* cycle number for a Si-CNT fabric electrode intentionally bent and prestressed to 25 MPa.

CNTs and lowers both the maximum elongation and the UTS of the CNT fabric.[54−56]

Si deposition onto the CNT fabric has little effect on the UTS but decreases its maximum elongation. While selected Si-coated CNT samples demonstrated UTS up to 150 MPa and maximum elongation up to 0.8%, the average values for the UTS and maximum elongations were ~100 MPa and 0.5%, respectively (Figure 5b). In the as-produced CNT fabric, the high maximum strain (Figure 5a) and the resultant high fracture toughness were achieved by the energy dissipation during continuous sliding of the van der Waals bonded individual tubes relative to each other. Due to the covalent nature of the atomic bonds in Si and its resultant brittle behavior, formation of continuous amorphous Si coating on the internal surface of the CNT fabric could be expected to significantly reduce its ductility, but the experimentally measured composite fabric ductility and the UTS (Figure 5b) were relatively high. Indeed, the non-uniformities observed within amorphous Si coatings (Figure 2b) and the pores within the Si-CNT fabric should act as pre-existing cracks, lowering both the ultimate strength and the maximum elongation achievable in such a composite. SEM studies of the fracture surface (Figure 6) revealed that the high UTS of the Si-CNT fabrics could be attributed to realignment and the pull-out behavior of CNTs. The fracture edge of the Si-CNT fabric specimens has a clear transition from the randomly oriented CNT fabric to highly aligned CNTs (Figure 6a,b). We expect that the degree of plastic deformation of the composite fabric could be greatly increased by using active materials of higher ductility than Si (such as Sn or Mg). We further hypothesize that reduction of the deposition temperature (Figure 5a) could favor achieving better mechanical properties.

Despite volumetric changes of Si during insertion and extraction of Li,[57,58] the mechanical properties of the Si-CNT fabric did not degrade significantly after cycling (Figure 5b), thus demonstrating multifunctional properties of the synthesized fabric. Both the UTS and

maximum elongation were reduced by only ~10%. The cycled Si-CNT fabric electrodes demonstrated similar pull-out behavior (Figure 6c,d). The retention of the fabric's mechanical properties could be a result of limiting the extent of Li insertion into the individual tubes (Figure 4b,c).

To further demonstrate the robustness of the Si-CNT fabric, the samples were statically loaded at 25 MPa prior to electrochemical testing. The prestressed Si-CNT fabrics also demonstrate good cycling stability with an average dealloying capacity of ~480 $mAh \cdot g^{-1}$ and good cycle stability (Figure 7).

High values of the achieved UTS combined with the low density of Si and C favor the use of the multifunctional Si-CNT fabrics in applications where high specific capacity (Table S2) and specific strength are essential. Indeed, the specific strength of the synthesized electrodes exceeds that of both Cu and Al, conventional current collectors for anodes and cathodes, respectively (Figure 5c). It further exceeds the specific strength of multiple Al alloys, Ti, cast iron, and even selected types of structural steel (Figure 5c).

CONCLUSION

In summary, we report the large-scale fabrication of CNT fabric coated with an active (Li-ion hosting) material for use as an electrode for multifunctional Li-ion batteries with high mechanical strength, flexibility, conductivities, and capacity coupled with good cyclability. The investigated example of Si-CNT fabric fabricated *via* vapor deposition routes demonstrated 2.5 times higher specific capacity than state of the art anodes and stable electrochemical performance for >150 cycles with the capability to retain over 90% of its original strength after cycling. The lightweight, good structural stability, and high electrical and thermal conductivities of CNTs may allow CNT fabrics to serve as a platform for the generation of novel flexible batteries with enhanced properties and functionalities. We expect that future studies with other active material coatings and deposition methods may allow us to further optimize their performance and achieve even better mechanical and electrochemical properties of the flexible CNT-based electrodes, contributing to the development of high-power, flexible, and structural batteries.

METHODS

Carbon nanotube material was produced by floating catalyst CVD with ethanol as the primary carbon source. Ferrocene dissolved in the fuel served as the source for iron catalyst particles. Sulfur was added as a catalyst conditioner. The fuel mixture was injected into the furnace in the presence of hydrogen. The vaporized fuel mixture is taken through carefully controlled thermal gradients to produce a narrow distribution of the proper size catalyst particles and to crack the ethanol to create a carbon source for the nanotubes. Nanotube growth continues through the furnace. Upon exiting the furnace hot zone, the CNT material is collected onto a moving belt or drum until the required dimensions are obtained. The CNT sheet is then extracted from the furnace and may be treated to enhance electrical and/or mechanical properties.

The nonwoven CNT fabric was cut into strips (100 mm × 25 mm) and into rounds (12.7 mm diameter) for testing in Li-ion pouch and 2016-type coin cells, respectively. The CNT fabrics were then coated with Si *via* low-pressure (600 mTorr) CVD of SiH_4 (5% in He balance; Airgas, USA) at 500 °C. The produced composite contained 47 ± 2% wt % Si. The Si and C contents were calculated using mass change measurements after Si deposition.

Micrographs of the material morphology and structure were taken by SEM (Hitachi S-4700, Japan). Images were taken with a 10 kV accelerating voltage and working distances of 5.6–8.0 mm. EDS mapping was performed at 20 kV. Raman spectroscopy (WITec Instruments Corp., Germany) was performed using a 785 nm laser, 50× objective, and 600 grating density with a 10 s integration time for 5 accumulations to identify chemical bonds associated with Si and C.

Surface characterization of the synthesized and annealed CNT fabrics was performed on a Thermo K-Alpha XPS (Thermo Scientific, USA) using Al Kα radiation. All tests were conducted under vacuum ($<10^{-8}$ Torr) with a 200 μm spot size and energy resolutions of 1 and 0.1 eV for the survey and the high-resolution elemental scans, respectively. An electron flood gun was used to minimize surface charging. TGA analysis was performed on a TA Instruments Q50 (TA Instruments, USA) between room temperature and 800 °C at 5 $°C \cdot min^{-1}$ in N_2 gas flow. All samples were dried in vacuum at 80 °C prior to TGA and XPS analysis.

Thermal conductivity was measured at room temperature using a Huskeflux THISYS (Huskeflux Thermal Sensors, The Netherlands) calibrated to operate without glycerol. Pyrex, brass, and copper standards were utilized for system calibration. The linear electrical resistivity was measured using a custom-built 4-point probe system. The outer probes applied a constant 1 mA current. The voltage was measured by the inner probes which are separated by 2.0 cm.

Electrochemical performance of the CNT fabric-based electrodes was evaluated in two-electrode cells. Prior to assembly in an Ar-filled glovebox (<1 ppm H_2O, O_2; Innovative Technologies, USA), all electrodes were treated at 70 °C in vacuum overnight. All electrodes were tested in an electrolyte composed of 1 M $LiPF_6$ dissolved in a mixture of dimethyl carbonate, diethyl carbonate, ethylene carbonate, and vinylene carbonate (Novolyte Technologies, USA).

Cyclic voltammetry measurements were performed using a multichannel Solartron potentiostat (Solartron Analytical, USA). The capacity was not limited in the cyclic voltammetry measurements. Charge/discharge testing was conducted on a multichannel Arbin potentiostat (Arbin Instruments, USA). After testing, cells were dealloyed at 1 V until the current was less than 5% of the C/5 current. The electrodes were removed from the pouch cells and rinsed with anhydrous dimethyl carbonate (Sigma Aldrich, USA) to remove residual $LiPF_6$ salt.

Tensile test specimens were cut using a Hermes LS500XL CO_2 laser (GravoTech, Inc., USA) to form 100 mm × 5 mm CNT fabric rectangular strips and the edges were visually inspected for cracks. Thickness measurements were made using a micrometer to control for variations in the fabric thickness and provide accurate stress measurements. After cutting, the samples were mounted on disposable aluminum mounts to avoid damage during loading on the test frame providing a gauge length of 60 mm. Tensile test measurements were conducted on a MTS Insight 2 test frame (MTS Systems Corporation, USA) using screw action vice grips with double-serrated faces in accordance with ASTM D882-10 and using a MTS 100N load cell sampling at 45 Hz. The electrodes were loaded in uniaxial tension at a strain rate of 10% $\cdot min^{-1}$

until failure. Electrodes stressed prior to charge/discharge cycling were loaded at a constant 25 MPa.

Conflict of Interest: The authors declare no competing financial interest.

Acknowledgment. We thank J.T. Lee for TGA analysis, N. Nitta for EDS analysis, and D. Lewis for conductivity measurements. The work was partially supported by AFOSR (Grant FA9550-09-1-0151). K.E. was supported by the Robert Shackelford Fellowship.

Supporting Information Available: Additional figures. This material is available free of charge *via* the Internet at http://pubs.acs.org.

REFERENCES AND NOTES

1. Anton, S. R.; Erturk, A.; Inman, D. J. Multifunctional Self-Charging Structures Using Piezoceramics and Thin-Film Batteries. *Smart Mater. Struct.* **2010**, *19*, 115021–115021.
2. Liu, P.; Sherman, E.; Jacobsen, A. Design and Fabrication of Multifunctional Structural Batteries. *J. Power Sources* **2009**, *189*, 646–650.
3. Sun, L.; Karanjgaokar, N.; Sun, K.; Chasiotis, I.; Carter, W. C.; Dillon, S. High-Strength All-Solid Lithium Ion Electrodes Based on $Li_4Ti_5O_{12}$. *J. Power Sources* **2011**, *196*, 6507–6511.
4. Thomas, J. P.; Qidwai, M. A. The Design and Application of Multifunctional Structure-Battery Materials Systems. *JOM* **2005**, *57*, 18–24.
5. Evanoff, K.; Khan, J.; Balandin, A. A.; Magasinski, A.; Ready, W. J.; Fuller, T. F.; Yushin, G. Towards Ultrathick Battery Electrodes: Aligned Carbon Nanotube-Enabled Architecture. *Adv. Mater.* **2012**, *24*, 533–537.
6. Kovalenko, I.; Zdyrko, B.; Magasinski, A.; Hertzberg, B.; Milicev, Z.; Burtovyy, R.; Luzinov, I.; Yushin, G. A Major Constituent of Brown Algae for Use in High-Capacity Li-Ion Batteries. *Science* **2011**, *334*, 75–79.
7. Magasinski, A.; Dixon, P.; Hertzberg, B.; Kvit, A.; Ayala, J.; Yushin, G. High-Performance Lithium-Ion Anodes Using a Hierarchical Bottom-Up Approach. *Nat. Mater.* **2010**, *9*, 353–358.
8. Chan, C. K.; Peng, H.; Liu, G.; Mcllwrath, K.; Zhang, X. F.; Huggins, R. A.; Cui, Y. High-Performance Lithium Battery Anodes Using Silicon Nanowires. *Nat. Nanotechnol.* **2008**, *3*, 31–35.
9. Kasavajjula, U.; Wang, C.; Appleby, A. J. Nano- and Bulk-Silicon-Based Insertion Anodes for Lithium-Ion Secondary Cells. *J. Power Sources* **2007**, *163*, 1003–1039.
10. Kim, H.; Cho, J. Superior Lithium Electroactive Mesoporous Si@Carbon Core−Shell Nanowires for Lithium Battery Anode Material. *Nano Lett.* **2008**, *8*, 3688–3691.
11. Park, M.-H.; Kim, M. G.; Joo, J.; Kim, K.; Kim, J.; Ahn, S.; Cui, Y.; Cho, J. Silicon Nanotube Battery Anodes. *Nano Lett.* **2009**, *9*, 3844–3847.
12. Wilson, A. M.; Way, B. M.; Dahn, J. R.; van Buuren, T. Nanodispersed Silicon in Pregraphitic Carbons. *J. Appl. Phys.* **1995**, *77*, 2363–2363.
13. Bridel, J. S.; Azais, T.; Morcrette, M.; Tarascon, J. M.; Larcher, D. Key Parameters Governing the Reversibility of Si/Carbon/CMC Electrodes for Li-Ion Batteries. *Chem. Mater.* **2010**, *22*, 1229–1241.
14. Guo, J. C.; Wang, C. S. A Polymer Scaffold Binder Structure for High Capacity Silicon Anode of Lithium-Ion Battery. *Chem. Commun.* **2010**, *46*, 1428–1430.
15. Mazouzi, D.; Lestriez, B.; Roue, L.; Guyomard, D. Silicon Composite Electrode with High Capacity and Long Cycle Life. *Electrochem. Solid-State Lett.* **2009**, *12*, A215–A218.
16. Hertzberg, B.; Benson, J.; Yushin, G. *Ex-Situ* Depth-Sensing Indentation Measurements of Electrochemically Produced Si-Li Alloy Films. *Electrochem. Commun.* **2011**, *13*, 818–821.
17. Evanoff, K.; Magasinski, A.; Yang, J.; Yushin, G. NanoSi-Coated Graphene Granules as Anodes for Li-Ion Batteries. *Adv. Energy Mater.* **2011**, *1*, 495–498.
18. Hertzberg, B.; Alexeev, A.; Yushin, G. Deformations in Si-Li Anodes upon Electrochemical Alloying in Nano-Confined Space. *J. Am. Chem. Soc.* **2010**, *132*, 8548–8549.
19. Inoue, Y.; Suzuki, Y.; Minami, Y.; Muramatsu, J.; Shimamura, Y.; Suzuki, K.; Ghemes, A.; Okada, M.; Sakakibara, S.; Mimura, F.; *et al.* Anisotropic Carbon Nanotube Papers Fabricated from Multiwalled Carbon Nanotube Webs. *Carbon* **2011**, *49*, 2437–2443.
20. Luo, S.; Wang, K.; Wang, J.; Jiang, K.; Li, Q.; Fan, S. Binder-Free $LiCoO_2$/Carbon Nanotube Cathodes for High-Performance Lithium Ion Batteries. *Adv. Mater.* **2012**, *24*, 2294–2298.
21. Wang, C.; Li, D.; Too, C. O.; Wallace, G. G. Electrochemical Properties of Graphene Paper Electrodes Used in Lithium Batteries. *Chem. Mater.* **2009**, *21*, 2604–2606.
22. Balandin, A. A. Thermal Properties of Graphene and Nanostructured Carbon Materials. *Nat. Mater.* **2011**, *10*, 569–581.
23. Lau, C.; Cervini, R.; Clarke, S.; Markovic, M.; Matisons, J.; Hawkins, S.; Huynh, C.; Simon, G. The Effect of Functionalization on Structure and Electrical Conductivity of Multi-Walled Carbon Nanotubes. *J. Nanopart. Res.* **2008**, *10*, 77–88.
24. Park, O.-K.; Jeevananda, T.; Kim, N. H.; Kim, S.-i.; Lee, J. H. Effects of Surface Modification on the Dispersion and Electrical Conductivity of Carbon Nanotube/Polyaniline Composites. *Scr. Mater.* **2009**, *60*, 551–554.
25. Li, Q. W.; Li, Y.; Zhang, X. F.; Chikkannanavar, S. B.; Zhao, Y. H.; Dangelewicz, A. M.; Zheng, L. X.; Doorn, S. K.; Jia, Q. X.; Peterson, D. E.; *et al.* Structure-Dependent Electrical Properties of Carbon Nanotube Fibers. *Adv. Mater.* **2007**, *19*, 3358–3363.
26. Tantang, H.; Ong, J. Y.; Loh, C. L.; Dong, X.; Chen, P.; Chen, Y.; Hu, X.; Tan, L. P.; Li, L.-J. Using Oxidation to Increase the Electrical Conductivity of Carbon Nanotube Electrodes. *Carbon* **2009**, *47*, 1867–1870.
27. Dahn, J. R.; Zheng, T.; Liu, Y.; Xue, J. S. Mechanisms for Lithium Insertion in Carbonaceous Materials. *Science* **1995**, *270*, 590–593.
28. Abouimrane, A.; Compton, O. C.; Amine, K.; Nguyen, S. T. Non-annealed Graphene Paper as a Binder-Free Anode for Lithium-Ion Batteries. *J. Phys. Chem. C* **2010**, *114*, 12800–12804.
29. Pan, D.; Wang, S.; Zhao, B.; Wu, M.; Zhang, H.; Wang, Y.; Jiao, Z. Li Storage Properties of Disordered Graphene Nanosheets. *Chem. Mater.* **2009**, *21*, 3136–3142.
30. Spahr, M. E.; Palladino, T.; Wilhelm, H.; Wursig, A.; Goers, D.; Buqa, H.; Holzapfel, M.; Novak, P. Exfoliation of Graphite during Electrochemical Lithium Insertion in Ethylene Carbonate-Containing Electrolytes. *J. Electrochem. Soc.* **2004**, *151*, A1383–A1395.
31. Yu, M. F.; Lourie, O.; Dyer, M. J.; Moloni, K.; Kelly, T. F.; Ruoff, R. S. Strength and Breaking Mechanism of Multiwalled Carbon Nanotubes under Tensile Load. *Science* **2000**, *287*, 637–640.
32. Park, J. G.; Smithyman, J.; Lin, C.-Y.; Cooke, A.; Kismarahardja, A. W.; Li, S.; Liang, R.; Brooks, J. S.; Zhang, C.; Wang, B. Effects of Surfactants and Alignment on the Physical Properties of Single-Walled Carbon Nanotube Buckypaper. *J. Appl. Phys.* **2009**, *106*, 104310–104310.
33. Pham, G. T.; Park, Y.-B.; Wang, S.; Liang, Z.; Wang, B.; Zhang, C.; Funchess, P.; Kramer, L. Mechanical and Electrical Properties of Polycarbonate Nanotube Buckypaper Composite Sheets. *Nanotechnology* **2008**, *19*, 325705–325705.
34. Zhang, X.; Sreekumar, T. V.; Liu, T.; Kumar, S. Properties and Structure of Nitric Acid Oxidized Single Wall Carbon Nanotube Films. *J. Phys. Chem. B* **2004**, *108*, 16435–16440.
35. Morris, R. S.; Dixon, B. G.; Gennett, T.; Raffaelle, R.; Heben, M. J. High-Energy, Rechargeable Li-Ion Battery Based on Carbon Nanotube Technology. *J. Power Sources* **2004**, *138*, 277–280.
36. Pushparaj, V. L.; Shaijumon, M. M.; Kumar, A.; Murugesan, S.; Ci, L.; Vajtai, R.; Linhardt, R. J.; Nalamasu, O.; Ajayan, P. M. Flexible Energy Storage Devices Based on Nanocomposite Paper. *Proc. Natl. Acad. Sci. U.S.A.* **2007**, *104*, 13574–13577.
37. Antunes, E. F.; Lobo, A. O.; Corat, E. J.; Trava-Airoldi, V. J.; Martin, A. A.; Verissimo, C. Comparative Study of First- and Second-Order Raman Spectra of MWCNT at Visible and Infrared Laser Excitation. *Carbon* **2006**, *44*, 2202–2211.

38. Tan, P.; Dimovski, S.; Gogotsi, Y. Raman Scattering of Nonplanar Graphite: Arched Edges, Polyhedral Crystals, Whiskers and Cones. *Philos. Trans. R. Soc., A* **2004**, *362*, 2289–2310.
39. Ferrari, A. C.; Robertson, J. Interpretation of Raman Spectra of Disordered and Amorphous Carbon. *Phys. Rev. B: Condens. Mattter Mater. Phys.* **2000**, *61*, 14095–14095.
40. Iqbal, Z.; Veprek, S. Raman Scattering from Hydrogenated Microcrystalline and Amorphous Silicon. *J. Phys. C: Solid State Phys.* **1982**, *15*, 377–377.
41. Nguyen, J. J.; Evanoff, K.; Ready, W. J. Amorphous and Nanocrystalline Silicon Growth on Carbon Nanotube Substrates. *Thin Solid Films* **2011**, *519*, 4144–4147.
42. Nozaki, T.; Yoshida, S.; Okazaki, K. Plasma-Induced Damage and Surface Functionalization of Double-Walled Carbon Nanotubes Using Atmospheric Pressure RF Discharge. *Plasma Processes Polym.* **2012**, 10.1002/ppap.201100218.
43. Yokoyama, D.; Iwasaki, T.; Ishimaru, K.; Sato, S.; Nihei, M.; Awano, Y.; Kawarada, H. Low-Temperature Synthesis of Multiwalled Carbon Nanotubes by Graphite Antenna CVD in a Hydrogen-Free Atmosphere. *Carbon* **2010**, *48*, 825–831.
44. Zhang, G.; Mann, D.; Zhang, L.; Javey, A.; Li, Y.; Yenilmez, E.; Wang, Q.; McVittie, J. P.; Nishi, Y.; Gibbons, J.; *et al.* Ultra-High-Yield Growth of Vertical Single-Walled Carbon Nanotubes: Hidden Roles of Hydrogen and Oxygen. *Proc. Natl. Acad. Sci. U.S.A.* **2005**, *102*, 16141–16145.
45. Dimov, N.; Kugino, S.; Yoshio, M. Carbon-Coated Silicon as Anode Material for Lithium Ion Batteries: Advantages and Limitations. *Electrochim. Acta* **2003**, *48*, 1579–1587.
46. Jung, H.; Park, M.; Han, S. H.; Lim, H.; Joo, S.-K. Amorphous Silicon Thin-Film Negative Electrode Prepared by Low Pressure Chemical Vapor Deposition for Lithium-Ion Batteries. *Solid State Commun.* **2003**, *125*, 387–390.
47. Bandhauer, T. M.; Garimella, S.; Fuller, T. F. A Critical Review of Thermal Issues in Lithium-Ion Batteries. *J. Electrochem. Soc.* **2011**, *158*, R1.
48. Chen, S. C.; Wan, C. C.; Wang, Y. Y. Thermal Analysis of Lithium-Ion Batteries. *J. Power Sources* **2005**, *140*, 111–124.
49. Maleki, H.; Hallaj, S. A.; Selman, J. R.; Dinwiddie, R. B.; Wang, H. Thermal Properties of Lithium-Ion Battery and Components. *J. Electrochem. Soc.* **1999**, *146*, 947–954.
50. Fleckenstein, M.; Bohlen, O.; Roscher, M. A.; Bäker, B. Current Density and State of Charge Inhomogeneities in Li-Ion Battery Cells with $LiFePO_4$ as Cathode Material Due to Temperature Gradients. *J. Power Sources* **2011**, *196*, 4769–4778.
51. Bonnefoi, L.; Simon, P.; Fauvarque, J. F.; Sarrazin, C.; Dugast, A. Electrode Optimisation for Carbon Power Supercapacitors. *J. Power Sources* **1999**, *79*, 37–42.
52. Shackelford, J. F.; Alexander, W. Mechanical Properties of Materials. In *CRC Materials Science and Engineering Handbook*, 3rd ed.; Shackelford, J. F., Alexander, W., Eds.; CRC Press: Boca Raton, FL, 2001.
53. Sun, Y.-P.; Fu, K.; Lin, Y.; Huang, W. Functionalized Carbon Nanotubes: Properties and Applications. *Acc. Chem. Res.* **2002**, *35*, 1096–1104.
54. Gojny, F. H.; Nastalczyk, J.; Roslaniec, Z.; Schulte, K. Surface Modified Multi-Walled Carbon Nanotubes in CNT/Epoxy-Composites. *Chem. Phys. Lett.* **2003**, *370*, 820–824.
55. Martel, R.; Shea, H. R.; Avouris, P. Rings of Single-Walled Carbon Nanotubes. *Nature* **1999**, *398*, 299–299.
56. Yakobson, B.; Avouris, P. Mechanical Properties of Carbon Nanotubes. In *Carbon Nanotubes*, Dresselhaus, M., Dresselhaus, G., Avouris, P., Eds.; Springer: Berlin, 2001; pp 287−327.
57. Boukamp, B. A.; Lesh, G. C.; Huggins, R. A. All-Solid Lithium Electrodes with Mixed-Conductor Matrix. *J. Electrochem. Soc.* **1981**, *128*, 725–729.
58. Obrovac, M. N.; Christensen, L. Structural Changes in Silicon Anodes during Lithium Insertion/Extraction. *Electrochem. Solid-State Lett.* **2004**, *7*, A93–A93.